Mon. Not. R. Astron. Soc. **348,** 1120–1134 (2004) doi:10.1111/j.1365-2966.2004.07413.x

# Study of variable stars in the MOA data base: long-period red variables in the Large Magellanic Cloud – II. Multiplicity of the period–luminosity relation

S. Noda,[1,2⋆] M. Takeuti,[3] F. Abe,[1] I. A. Bond,[4] R. J. Dodd,[5,6,7] J. B. Hearnshaw,[8] M. Honda,[9] M. Honma,[10] J. Jugaku,[11] Y. Kan-ya,[10] Y. Kato,[1] P. M. Kilmartin,[5,8] Y. Matsubara,[1] K. Masuda,[1] Y. Muraki,[1] T. Nakamura,[12] K. Ohnishi,[13] M. Reid,[7] N. J. Rattenbury,[5] To. Saito,[14] Y. Saito,[1] H. Sato,[15] M. Sekiguchi,[9] J. Skuljan,[8] D. J. Sullivan,[7] T. Sumi,[1,16] R. Yamada,[1] T. Yanagisawa,[17] P. C. M. Yock[5] and M. Yoshizawa[18]

[1]*Solar-Terrestrial Environment Laboratory, Nagoya University, Nagoya 464-8601, Japan*
[2]*Astronomical Data Analysis Centre, National Astronomical Observatory, Mitaka 181-8588, Japan*
[3]*Astronomical Institute, Tohoku University, Sendai 980-8578, Japan*
[4]*Institute of Astronomy, University of Edinburgh, Royal Observatory, Edinburgh*
[5]*Department of Physics, University of Auckland, Auckland, New Zealand*
[6]*Carter National Observatory, PO Box 2909, Wellington, New Zealand*
[7]*School of Chemical and Physical Sciences, Victoria University, Wellington, New Zealand*
[8]*Department of Physics and Astronomy, University of Canterbury, Christchurch, New Zealand*
[9]*Institute for Cosmic Ray Research, University of Tokyo, Kashiwa, 277-8582, Japan*
[10]*VERA Project Office, National Astronomical Observatory, Mitaka 181-8588, Japan*
[11]*Institute for Civilization, Tokai University, Japan*
[12]*Department of Physics, Kyoto University, Kyoto 606-8502, Japan*
[13]*Nagano National College of Technology, Nagano 381-8550, Japan*
[14]*Tokyo Metropolitan College of Aeronautics, Tokyo 140-0011, Japan*
[15]*Research Institute of Fundamental Physics, Kyoto University, Kyoto 606, Japan*
[16]*Department of Astrophysical Science, Princeton University, Peyton Hall, Princeton, NJ 08544, USA*
[17]*National Aeronautical Laboratory of Japan, Space Research Technology Centre, 7-44-1, Chofu 182-8522, Japan*
[18]*Department of Fundamental Astrometry, National Astronomical Observatory, Mitaka 181-8565, Japan*

Accepted 2003 November 6. Received 2003 October 31; in original form 2002 September 25

**ABSTRACT**

Data for 4.4 million stars from the Microlensing Observations in Astrophysics (MOA) project are compared with the near-infrared data of the Deep Near Infrared Southern Sky Survey (DENIS). More than 4000 stars observed in both projects show a quite periodic light curve. Among them, a number of stars are likely eclipsing variables, and the others seem to be pulsating stars. The $K_S$ magnitudes of these red variables are in the range 10–12.5 but a minor clump at $K_S \approx$ 12.2 mag is also found. The multiplicity of the period–luminosity relation is confirmed, but most of the regular, large-amplitude variables are found on the relation established for the Mira stars. We study the properties of the variables on the colour–magnitude diagram constructed with the MOA red band $R_m$ and $K_S$ of DENIS. Multiplicity of the period–luminosity relation is briefly discussed in relation to the excitation mechanism of red pulsating variables.

**Key words:** catalogues – stars: AGB and post-AGB – stars: oscillations – stars: variables: other – Magellanic Clouds.

## 1 INTRODUCTION

Mira stars and semiregular variables are some of the brightest objects in galaxies and suppliers of dust and heavy elements by their strong mass-losing processes. These stars are thus important to investigate the chemical evolution of galaxies and Mira stars are also useful distance indicators. In spite of such an importance in astrophysics, the details of their evolutionary history and the mechanism of stellar pulsation have not yet been fully explained.

⋆E-mail: sachi.t.noda@nao.ac.jp

One of the most important features of Miras and semiregular (SR) stars found from the recent large-scale photometry of the Large Magellanic Cloud (LMC) is the multiplicity of the period–luminosity relation. Wood et al. (1999) pointed out the existence of five parallel sequences using the data base produced by the Massive Compact Halo Object (MACHO) Collaboration, and Wood (2000) studied the properties of the stars with *K*-band follow-up data. Recently, Cioni et al. (2001) confirmed such a multiplicity based on the data base of Experience pour la Recherche d'Objets Sombres (EROS), which is one of the large-scale photometry groups. The Microlensing Observations in Astrophysics (MOA) group also studied the properties of long-period red variables using their data base obtained with large-scale photometry (Noda et al. 2002, hereafter Paper I). Lebzelter, Schultheis & Melchior (2002) confirmed the three sequences from the AGAPEROS catalogue and the counterparts of the other groups.

The large-scale photometry originally designed to detect unseen bodies in the Universe through the microlensing effect uses a very broad bandpass optical system. Such a system is not adequate to measure the energy emitted by red stars whose energy distribution peaks in the near-infrared (NIR) domain. Therefore, NIR data are necessary to study the period–luminosity relation of the long-period red variables. One of the convenient NIR data bases for the Magellanic Clouds is the Deep Near Infrared Survey (DENIS) Catalogue toward the Magellanic Clouds (DCMC; Cioni et al. 2000a). In the present paper, the stars of the MOA data base are compared with the DCMC. The multiplicity of the period–luminosity relation of the LMC red variables was confirmed (Section 3). The changes of the period were observed for several stars (Section 4). The stars of different sequences have been found in the same area on the colour–magnitude diagram (CMD), but a shorter-period sequence was located at the bluer side (Section 5). The photometric properties of oxygen-rich and carbon-rich stars and the nature of long-period red variables are briefly discussed (Section 6).

## 2 IDENTIFICATION OF THE MOA DATA WITH DENIS

The MOA observations have used a new camera, MOA-cam2, since 1998 August (see Yanagisawa et al. 2000). In the present paper, we analysed 4.4 million stars in the LMC which have been observed for 2.3 yr, 840 d, from 1998 August to 2001 January. The positions of the MOA stars were compared with those in the DCMC. Only the objects identified with one entry in each catalogue were considered (313 706 stars – level 1 of selection criteria).

Among these stars, we selected 67 107 objects which were observed in the $K_S$ band. The colour $\langle V_m\rangle$–$\langle R_m\rangle$ and the $\langle R_m\rangle$ magnitude of these objects are indicated in Fig. 1. Magnitude in brackets indicates the mean brightness of each star, where $V_m$ and $R_m$ are the magnitudes of the visual and red passbands of the MOA observation.

The diagram is similar to the CMD of 261 805 stars drawn with the MACHO data base Alcock et al. (2000). Because their diagram was described with *V* and *R* in the Kron–Cousins system converted from their broad-band photometry, the similarity is limited to the main features. In Fig. 1, three bright vertical bands at $\langle V_m\rangle$–$\langle R_m\rangle \approx$ 0.1, 0.4 and 0.8–0.9 mag correspond to the main sequence of the LMC, foreground Galactic disc stars, and the red supergiants of the LMC, respectively.

The stars found at the position of ($\langle V_m\rangle$–$\langle R_m\rangle$) $\approx$ 0.6 mag and $\langle R_m\rangle \approx$ 18–19 mag (see Paper I, fig. 2) are horizontal-branch (HB), red clump and asymptotic giant branch (AGB) bump stars. These stars are below the detection limit of DENIS. The stars redder than

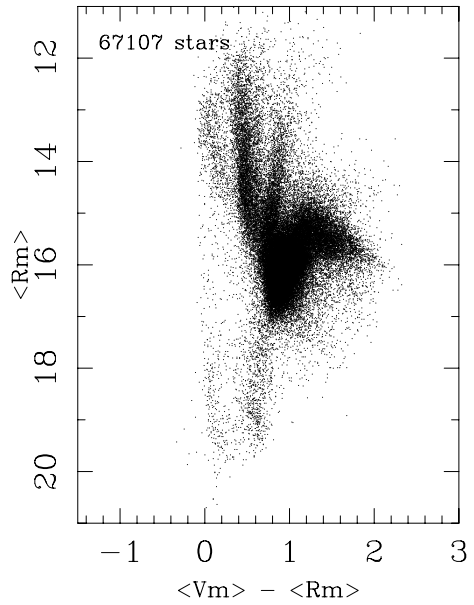


**Figure 1.** CMD ($\langle V_m\rangle$–$\langle R_m\rangle$ versus $\langle R_m\rangle$) of 67 107 sources observed by MOA and with the DCMC counterpart. The main concentrations of stars are explained in the text.

($\langle V_m\rangle$–$\langle R_m\rangle$) $\approx$ 1.2 mag are AGB stars above the tip of the red giant branch (TRGB) located at $\langle R_m\rangle \approx$ 16 mag.

Fig. 2 shows the CMD ($\langle R_m\rangle$–$K_S$) for the same sources. The LMC main sequence and the Hertzsprung gap correspond to the strips near ($\langle R_m\rangle$–$K_S$) $\approx$ 0–1 and 1–3 mag, respectively. The LMC supergiants extend upward to the red side of the foreground stars. These stars are brightest in the $K_S$ band. The observed $K_S$ magnitude of the TRGB is 11.98 mag for the LMC (Cioni et al. 2000b). The AGB extends from here to brighter and redder direction. Many stars scatter at the red side of the RGB and the AGB. Details of the (*V*–*R*, *V*) and NIR

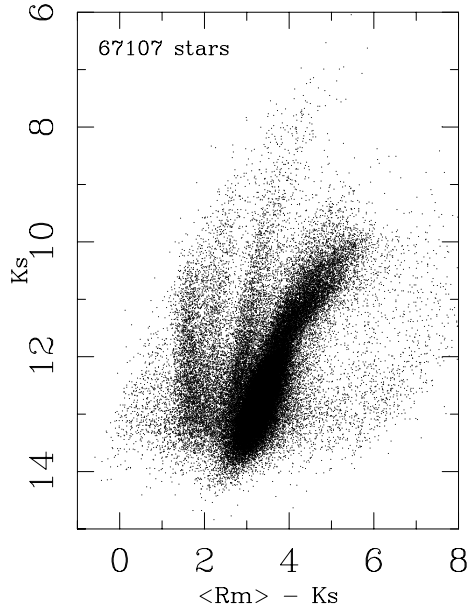


**Figure 2.** CMD ($\langle R_m\rangle$–$K_S$) versus $K_S$ of the LMC stars indicated in the preceding diagram. The horizontal axis is the colour derived from the mean red magnitude, $\langle R_m\rangle$ and single-epoch observations at the $K_S$ band. The vertical axis is $K_S$ mag. The strips of stars extending upward are explained in the text.

CMDs of the LMC have been discussed by van der Marel & Cioni (2001).

## 3 RED VARIABLES

### 3.1 Selection and period determination

From the stars found in both DCMC and MOA data bases, we selected variable stars with the following procedure.

(i) The stars which had a sufficient number of good quality measurements were selected from 313 706 stars in the preceding section. In the worst case, only 33 measurements were available from observations on 475 nights. More than 300 measurements were available in the best cases. Amongst 313 706 stars, 301 419 stars passed through this cut (level 2).

(ii) We selected the stars whose light variations exceeded the fluctuation possibly caused from the inaccuracy in the observations and reduction. The reduced $\chi^2$ check was applied to the measurements of each star to remove the stars whose fluctuation shows an almost Gaussian distribution. A total of 109 390 stars, whose reduced $\chi^2$ belonged to the upper 15 per cent, were selected (level 3).

(iii) The programming code, PDMM (phase dispersion minimization method for MOA), optimized for the large-scale photometry, was used to obtain the period and amplitude of the light curves, the same as for Paper I. The fluctuation from the assumed light curve was expressed by the parameter $\theta$, which should be equal to 1 for light variation without any periodicity and close to zero for light variation without any scattering. We denote $\theta$ for $V_{\rm m}$ by $\theta_V$ and for $R_{\rm m}$ by $\theta_R$.

(1) To detect the variable stars we assumed the trial period $P_k$ to be 0.1, 0.2, ..., 0.9, 1.0, 2.0, ..., 9.0, 10, 20, ..., 600, 700, 800 d. Then we removed the stars with $\theta_R > 0.9$ and $\theta_V > 0.95$ for $P_k > 700$ d. The threshold was lowered for the stars whose $P_k$ was shorter than 700 d. As a result many non-periodic variables and non-variable stars were removed. After this cut, 37 645 stars remained (level 4).

(2) We applied the PDMM to the stars selected after the preceding step with the trial period starting from 0.1 d and going to 840 d. The interval of 0.1 d was used. The stars with $\theta_R > 0.8$ for $P_k < 700$ d and $\theta_R > 0.9$ for $P_K > 700$ d were omitted. The distribution of $\theta_B$ for $P_k$ was very similar to $\theta_R$. A total of 36 841 stars remained after this selection (level 5).

(iv) The light curves of the remaining stars from the above criteria were investigated by careful eye-estimate. The non-variable stars that passed the preceding cuts by including one or more extraordinarily bright points, probably caused from the incompleteness of the reduction processes, were omitted. The variable stars whose period would be longer than 1000 d or more were also omitted. After removing such non-variables and seemingly too-long-period variables, we were left with 10 495 variable stars. 72 per cent of the sample that passed through the automatic selection process were not periodic variable stars (level 6).

(v) Because the PDMM gives small $\theta$ when the trial period is near the maximum time range of the MOA observations, we analysed the data again with a trial period of 30 d shorter. The interval of $P_k$ was set as 0.001 d. After omitting the stars with $\theta_R$ or $\theta_B$ greater than 0.9, we had 7310 stars (level 7).

(vi) The phase curves of the 7310 stars were checked by eye, referring to $\theta$ for the appropriate period. We still found 516 stars showing no periodicity. It was difficult to find any definite period in the light curves of 1369 stars because of their multiperiodic nature. Thus, the period was finally obtained for 5425 stars (level 8).

**Table 1.** Classification of light curves.

| Type | Number of stars | With $K_{\rm S}$ data | Remarks |
|---|---|---|---|
| S | 3371 | 2751 | Sinusoidal curve |
| W | 135 | 73 | Cepheid-like |
| C | 363 | 289 | Sharp light minimum |
| T | 989 | 854 | RV Tauri star-like |
| E | 567 | 395 | Eclipsing variable-like |

The light curves were then divided into five types: S, W, C, T and E. Examples are given in Appendix A. Type S shows a light curve very close to a sinusoidal curve (see Fig. A1); type W is characterized by a steep increase and mild decrease, just as observed for classical Cepheids (see Fig. A2); type C shows almost sinusoidal light curves but with sharp light minima (see Fig. A3); type T is characterized by twin peaks or alternating deep and shallow light minima, observed for the RV Tauri stars (see Fig. A4); and type E shows sharp light minima and with a flat bright portion typical of eclipsing variables (see Fig. A5). The number of stars in each type is given in Table 1. Of these 5425 stars, the $K_{\rm S}$ magnitude is present for 4362 stars. In the present classification, more than 60 per cent of the variables are type S stars.

Among these types, type C is unique in the variable star classification. Such a light curve has never been studied in other papers, so that the nature of these stars remains uncertain. The sharp light minimum of the light curve suggests a partial eclipse, but no clear out-of-eclipse phase was found. Until a more detailed study is made, these stars would be regarded as a subtype of pulsating stars. The three other types, S, W and T, were established as pulsating stars. It is worth noting that so many RV Tauri-like stars with the period longer than 150 d, which is the classical upper limit for the RV Tauri stars, were found. We excluded type E stars because their single colour light curves showed features of eclipsing binaries, and our study focuses on pulsating stars.

We show the $K_{\rm S}$ magnitude distribution of stars in Fig. 3. The dashed line indicates the histogram of 67 107 LMC stars including

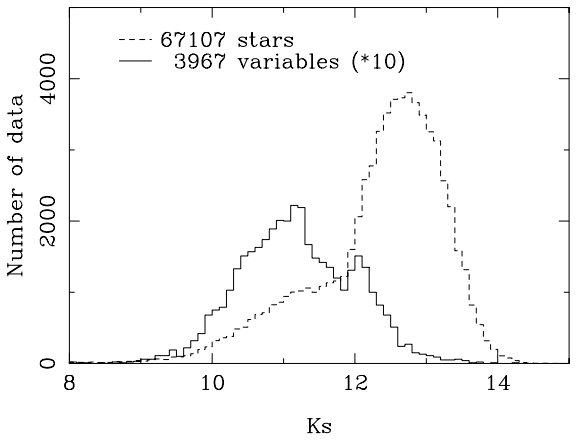


**Figure 3.** $K_{\rm S}$ magnitude of stars. The dashed histogram is the distribution of 67 107 LMC stars including non-variables. The solid histogram indicates 3967 pulsating stars, and it is drawn multiplying by 10 the star count. A major clump is found at 11.2 mag, and a minor clump is at 12.2 mag in the solid one.

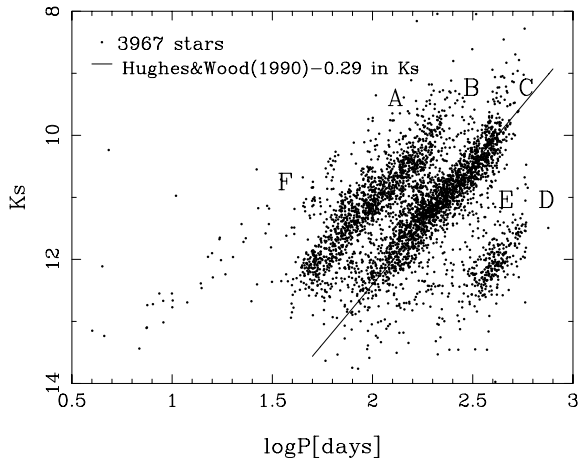


**Figure 4.** Period–luminosity (log $P, K_S$) diagram of the LMC red variables. A total of 3967 LMC variable stars are plotted. The strips found by Wood et al. (1999), and Wood (2000), partly confirmed by Cioni et al. (2001), are shown. The letters indicate difference sequences explained in the text.

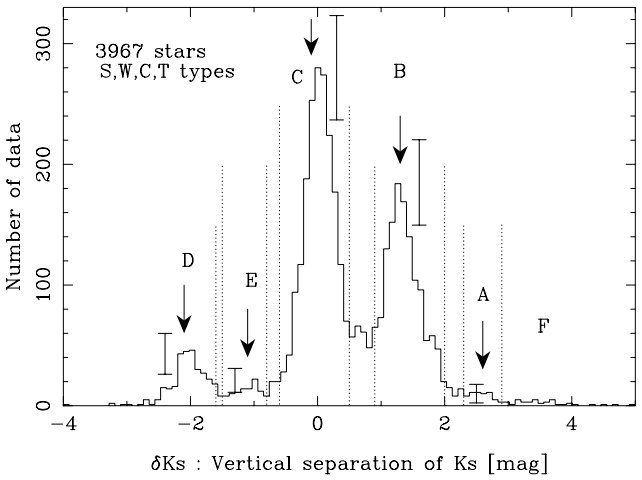


**Figure 5.** Deviation of the $K_S$ magnitude ($x$-axis) of variable stars from the sequence of O-rich Mira stars (see text). The dotted vertical lines define the group of the sequence of variables. The vertical segments indicate the error bar which is the square root of the star number included in the group.

non-variables. The detection limit of the DCMC for the $K_S$ magnitude is 14 mag, but the stars fainter than 12.7 are less abundant (Cioni et al. 2000a estimate the completeness limit of the DCMC at $K_S = 12.75$ in the LMC). The solid line indicates 3967 pulsating stars multiplied by 10 to facilitate the comparison. In this histogram a major clump is found at 11.2 mag, and a minor clump at 12.2 mag is clearly indicated. The major clump corresponds to the bump on the bright side of the dashed histogram (variables and non-variables).

### 3.2 Period–luminosity diagram

The common classification of variable stars divides long-period variables into Mira stars and SR variables. The General Catalogue of Variable Stars (GCVS; Kholopov 1985) defined these stars based on the amplitude of their light curves. The red intrinsic variables whose period is longer than 30 d, with the amplitude greater than 2.5 mag in the visual band, are the Mira stars, and the stars with amplitude smaller than 2.5 mag are classified as the SRs. The Miras have regular periodic light curves, while the SRs are characterized by less regular variability in the historical description. Regular SR stars are SRa, and less regular SRs are SRb. Because the amplitude of the light curves depends on the effective wavelength of the observations, we do not know where the threshold is between the Miras and the SRs before a detailed analysis.

The period–luminosity diagram of the 3967 pulsating stars is shown in Fig. 4. The strip pattern indicated in Wood et al. (1999) and Wood (2000), and then confirmed partly by Cioni et al. (2001), is clearly found. The period–luminosity relation of oxygen-rich Mira stars derived by Hughes & Wood (1990) is

$$K_0(\mathrm{mag}) = -3.86(\log(P) - 2.4) + 11.5, \quad (1)$$

where $P$ is the period in days and $K_0$ is the magnitude in the $K$ band corrected for extinction. This is very similar to the period–luminosity relation of Feast et al. (1989). The solid line shows the Hughes & Wood relation shifted upward by 0.29 mag, i.e.

$$K_S = -3.86(\log(P) - 2.4) + 11.21. \quad (2)$$

Fig. 5 shows the deviation $\delta K_S$ of the stars from the luminosity calculated by equation (2) for the observed period $P$.

The most abundant strip is the sequence of Mira stars. Five other peaks of the histogram are also found. Starting from the longest period they correspond to the sequence labelled D, E, C, B and A in Wood et al. (1999). Sequence F is the shortest period. The properties of the six sequences are given in the following. Their locations are given with respect to sequence C.

**Sequence A:** The stars whose $\delta K_S$ was in the range from 2.3 to 2.9 mag were treated as members of sequence A. The stars were 2.5 mag brighter or 0.66 dex shorter in log $P$ (d) than the oxygen-rich Miras. There were 59 stars in this sequence. The mean brightness of these stars was $K_S(\mathrm{mag}) \approx 10.5$. Cioni et al. (2001) did not detect this group.

**Sequence B:** The stars whose $\delta K_S$ was in the range from 0.9 to 2.0 mag were treated as members of sequence B. The stars were 1.3 mag brighter or 0.34 dex shorter in log $P$ (d) than the oxygen-rich Miras. There were 1253 stars in this sequence. The mean brightness of these stars was $K_S(\mathrm{mag}) \approx 11.0$. The stars classified as Group B in Paper I belong to this sequence.

**Sequence C:** The stars whose $\delta K_S$ was in the range from $-0.6$ to 0.5 mag were treated as members of sequence C. The stars belong to the sequence of oxygen-rich Miras. There were 1867 stars in this sequence. The mean brightness of these stars was $K_S(\mathrm{mag}) \approx 11.0$, the same as sequence B. The stars classified as Group A in Paper I belong to this sequence.

**Sequence D:** The stars whose $\delta K_S$ was in the range from $-1.5$ to $-0.8$ mag were treated as members of sequence D. The stars were 2.0 mag fainter or 0.52 dex longer in log $P$ (d) than the oxygen-rich Miras. There were 286 stars. The mean brightness of these stars was $K_S(\mathrm{mag}) \approx 12.2$, fainter than those of sequence C.

**Sequence E:** The stars whose $\delta K_S$ was in the range from $-1.5$ to $-0.8$ mag were treated as members of sequence E. The stars were 1.1 mag fainter or 0.28 dex longer in log $P$ (d) than the oxygen-rich Miras. The sequence contained 99 stars. The mean brightness of these stars was $K_S(\mathrm{mag}) \approx 12.2$, clearly fainter than for sequence C. Sequences D and E formed the fainter clump of Fig. 3.

**Sequence F:** We called the stars with $\delta K_S$ in the range from 3.0 to 4.0 mag sequence F. The stars were 1 mag brighter than sequence A. There were 30 stars in this sequence.

**Outside sequence F:** Ten stars with $\delta K_S$ greater than 4.0 mag were found.

Sequence F is located in the Hertzsprung gap, and it is not populated by red giant stars. The typical position of classical Cepheids

**Table 2.** Sequences of red variables in the LMC.

| Sequence | Number of stars | Remarks |
|---|---|---|
| A | 59 | 2.5 mag brighter than sequence C |
| B | 1253 | 1.3 mag brighter than sequence C |
| C | 1867 | Containing many oxygen-rich Miras |
| D | 286 | 2.0 mag fainter than sequence C |
| E | 99 | 1.1 mag fainter than sequence C |

on the period–luminosity diagram is $K = 11.1$ mag for $\log P\,(\mathrm{d}) = 1.5$ (Laney & Stobie 1994); Gieren, Fouqué & Gomez 1998). This is just the position of sequence F. Cioni et al. (2001) classified the stars corresponding to sequence F as classical Cepheids. We do not investigate sequence F in this paper.

The number of stars in each sequence (A–E) is tabulated in Table 2. Among the five sequences in the period–luminosity diagram, 88 per cent of our sample belong to sequences B and C. The stars of these sequences form the main clump of Fig. 3.

The positions of Galactic Mira stars on the period–luminosity diagram were studied by Bedding & Zijlstra (1998) with the data of the *Hipparcos* mission. Comparing their results with the present sequences, we assume that T Cep, o Cet and R Leo are on sequence C, and R Cas and $\chi$ Cyg on sequence D. R Car looks like a member of sequence E. The Galactic SRs in their paper are likely to be members of sequences B and C.

### 3.3 Ambiguity of the period

It should be noted that the tabulated period of MOA J051607.7−694425, denoted as nlmc1-239264, was 129.5 d in Paper I. However, a period of 255.4 d is adopted in the present analysis. The difference comes from only one data point. The data indicated a light maximum corresponding to the period of 129.5 d, but no such maximum was found in the present study. The star belongs to sequence C when the present period is adopted, but belongs to sequence B in the previous study. However, the amplitude of this star is larger than the other members of group B of Paper I. The ambiguity of the period determination affects the membership of the star to a given sequence.

In our period determination process, two types of ambiguities could result in an incorrect period.

**Case 1:** An insufficient coverage of the light curve gives a less reliable period.

**Case 2:** A period-doubling-like feature in the light variation affects the period determination. This feature known in the non-linear dynamics is characterized with the alternate high and low light maxima and/or the alternate deep and shallow minima. Sometimes the light curves of RV Tauri stars are discussed as the favourite examples of such a feature. In the study of these stars, the time interval between two successive light maxima is called the single period, and twice this single period is called the formal period. The PDMM sometimes picked up the single period, and sometimes the formal period. Examples are shown in Appendix B.

The light curves mentioned in case 2 are similar to the oscillatory motion also known as the Period 2 oscillation in discrete dynamics. The Period 2 oscillation is the first step of the period-doubling bifurcation process that appeared in the hydrodynamic studies of stellar pulsation for low-surface gravity models (see Buchler & Kovács 1987). Recent papers show that in RV Tauri stars the nature of the period-doubling feature is the 1 : 2 resonance of a strongly enhanced mode and a strongly dissipative mode, not the Period 2 oscillation (see, for example, Buchler & Kolláth 2001, and also see Kolláth 1998).

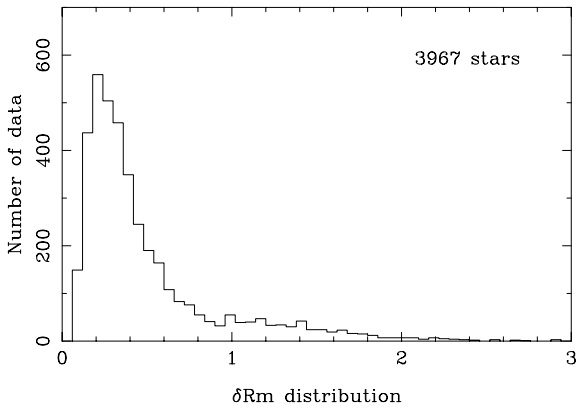


**Figure 6.** Distribution of the amplitude $\delta R_{\mathrm{m}}$. The extended slope beyond the amplitude $\delta R_{\mathrm{m}} \approx 0.9$ mag indicates the Mira stars in the classical view.

### 3.4 Amplitude distribution

The nature of the multiple period–luminosity relation is elucidated through careful studies of the observational properties, such as the amplitude and the periodicity. The distribution of the amplitude $\delta R_{\mathrm{m}}$ of stars is shown in Fig. 6. $\delta R_{\mathrm{m}}$ is defined as the amplitude of the light curve in the MOA red band ($R_{\mathrm{m}}$). The extended slope of the amplitude $\delta R_{\mathrm{m}}$ beyond 0.9 mag indicates classical Mira stars. As the number of stars studied in this work is considerably larger than in Paper I, the number of small-amplitude variables has increased. The number of large-amplitude stars has also increased. This may make it easier to distinguish the Mira stars.

Cioni et al. (2001) presented the amplitude distribution in fig. 4 of their paper. The pattern is similar to ours, but their amplitude is larger than ours. This may be caused by the difference in measuring the amplitude. In our study, the amplitude was given as the difference between the mean magnitude of the brightest and faintest bins in the PDMM analyses. This gave smaller values compared with the difference between the magnitudes at the light maximum and light minimum. It is plausible that the present results could be identical with theirs.

Cioni et al. (2001) also suggested the presence of a dip at the amplitude of 0.9 mag in $R_{\mathrm{E}}$, the red magnitude in the EROS observations, that is likely to be the threshold between the Mira stars and SR variables. In Fig. 6 we have found a shallow unclear dip at $\delta R_{\mathrm{m}} \approx 0.95$ mag. In the amplitude distribution of $I$ magnitude, no clear dip corresponding to the boundary between the Mira stars and SR variables was found (Whitelock 1999). Although our results did not give any definite answer whether or not red long-period variables consist of two different groups according to their amplitude, if we adopt 0.9 mag as the threshold, most of the 146 stars studied in Paper I are Mira stars and members of Group B are SR variables just like sequence B in the present work.

The distribution of the amplitude $\delta R_{\mathrm{m}}$ for each sequence is indicated in Fig. 7. Sequence A contains no large-amplitude stars, while in sequence B only five stars whose amplitude is larger than 1 mag are found. In sequence C many large-amplitude stars are found. For 99 stars of sequence E, 17 stars show an amplitude larger than 1 mag. Sequence D contains only one star whose amplitude is larger

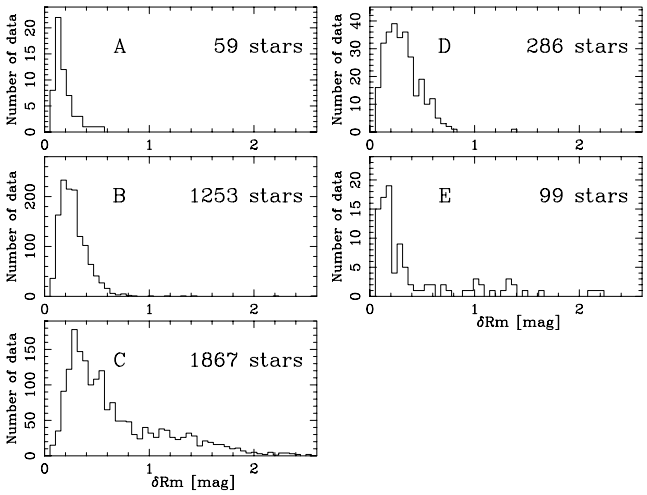


**Figure 7.** Distribution of the amplitude $\delta R_{\rm m}$ of the stars in each period–magnitude sequence. A–E correspond to sequences A–E, respectively.

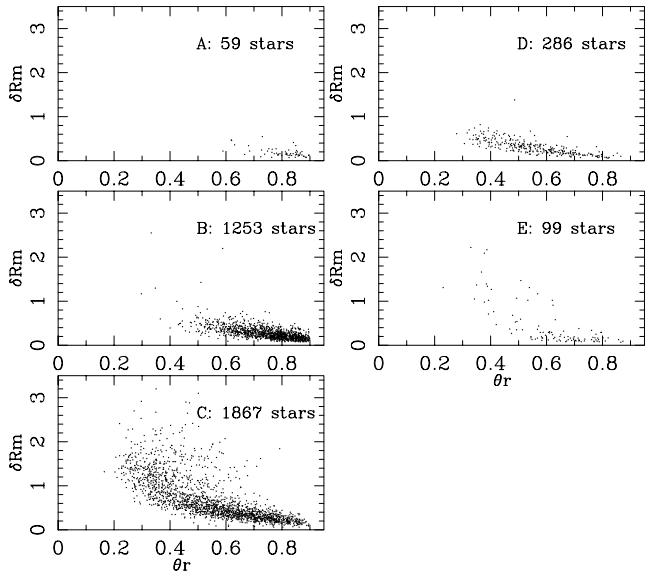


**Figure 9.** Relation between the regularity and the amplitude. The horizontal axis is the parameter $\theta_R$, the criterion of regularity, of the PDMM code. The vertical axis is the amplitude $\delta R_{\rm m}$. Each panel shows the relation for each sequence. Most of the large-amplitude and regular variables are found in sequence C.

than 1 mag. The period of the large-amplitude stars in sequences B and E is discussed in Appendix B.

### 3.5 Periodicity of each sequence

The parameter $\theta_R$ from the PDMM can be used to evaluate the regularity of the variability (Fig. 8). In the present analysis, the smallest values of $\theta_R$ are approximately 0.2, and the values of $\theta_R$ are 0.7–0.8 for typical SR variables. The members of sequence A are SR variables because their $\theta_R$ are larger than 0.6 (the smallest $\theta_R = 0.59$). For the majority of the members of sequence B, $\theta_R$ is larger than 0.6. $\theta_R$ for the members of sequence C distribute over the whole $\theta_R$ range in the diagram. In sequence D, the smallest values of $\theta_R$ are approximately 0.3 and the distribution is similar to sequence C. The distributions of sequence E are also similar to those of sequence C.

The regularity of each of the sequences shows that sequence C consists of Miras and SRs, just the same as the results from the distribution of the amplitudes. In fact, $\theta_R$ and $\delta R_{\rm m}$ indicated in Fig. 9 show that the large-amplitude regular variables defined as Miras are found in sequences B, C and E, but especially in sequence C. In sequence D, only one such star was found, as stated in the previous subsection. There are no Mira stars in sequence A. The stars with $\delta R_{\rm m}$ less than approximately 0.9 are located on the straight line which starts from the bottom-right corner. It is shown that lower amplitude stars are less periodic. Such a property is likely to be the stochastic enhancement of pulsation. In Cioni et al. (2001), sequence B and the majority of sequence C are formed by SRa stars, while SRb stars are common in sequence D. Because we have concentrated on the study of regular variables, we do not discuss the abundance of SRb stars in each sequence.

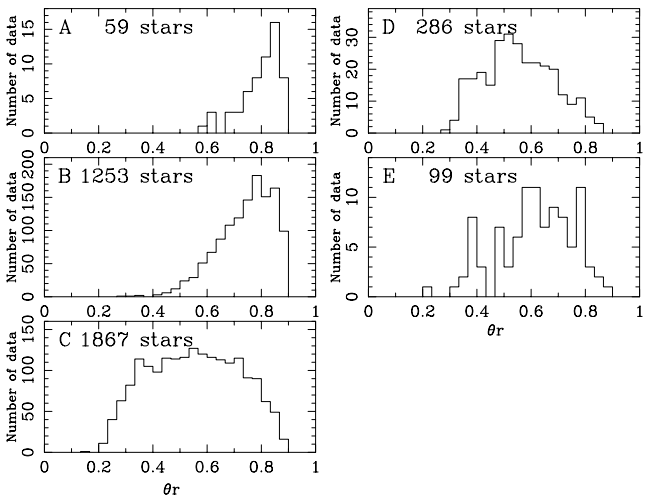


**Figure 8.** Regularity $\theta_R$ of the stars in each period–magnitude sequence. A–E indicate sequences A–E, respectively.

### 3.6 Multiplicity of the period–luminosity relationship

The five sequences found using the MACHO data base have been confirmed with the MOA data base. It is clarified that the richest sequence, sequence C, contains mostly Mira stars. Many SR variables also belong to this sequence. Two brighter sequences, sequences A and B, consist mostly of SR variables. Although the nature of the fainter sequences is ambiguous, the majority of the members are also SR variables.

We examined the space distribution of each sequence. Fig. 10 indicates the source density in constant bins. We found that the most abundant region slightly inclines toward the north of the LMC centre. Compared with sequences A, B and C, the concentration of sequences D and E to the LMC centre is weak. Although the stars in sequence D and E are very few, such a difference suggests a difference in their nature. Low-mass stars which evolve to the TRGB (Alcock et al. 2000) are old stars and widely spread spatially. The spatial distribution of sequence D and E stars indicates that they are on the RGB.

The comparison of the period–luminosity relations of the solar neighborhood Miras and the LMC Miras is still difficult because the absolute magnitude is studied for only a limited number of Miras. Six Galactic Miras studied in Bedding & Zijlstra (1998) belong to sequences C, D, and E, while many SRs were found at the position

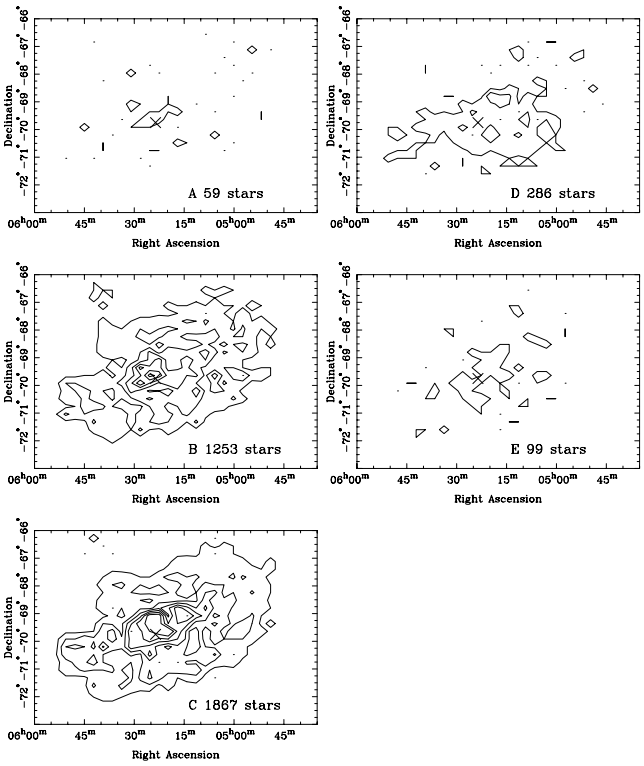


**Figure 10.** The source density of the stars in each period–magnitude sequence (A–E).

of sequences B and C. No strip structure was confirmed for the red variables in the Galactic bulge (Alard et al. 2001). In the present investigation, it is probable that most of the Mira stars belong to sequence C.

## 4 PERIOD TRANSITION

We compared our periods determined in the present study with those of Hughes & Wood (1990) and found disagreements for seven stars (Table 3). These light curves in the present MOA data base have good signal-to-noise (S/N), cover long period, and do not show multiperiod, therefore our periods should be correct.

If such a difference is caused by actual period change (i.e. period transition), the location of the star in the period–luminosity diagram also changes. The fifth column in Table 3 indicates the movements between the sequences. For example, the star J053005.8−702407 was located on sequence C according to the period of Hughes & Wood (1990), while it is located on sequence B in our analysis. The star J051709.4−695927 remains in the same sequence (C). Note that, because we used the single epoch observation in $K_S$, the identification of the sequence remains uncertain. To investigate the position of each star, multiphase photometric data in the NIR wavelengths are necessary.

**Table 3.** Period transition of stars. $P_{SHV}$ (in d) is the period in Hughes & Wood (1990). $P$ (in d) is the period from the present analysis. Sequence indicates the sequence on which the star is located according to the period by Hughes & Wood (1990)/by the current analysis.

| Star (MOA) | $P_{SHV}$ | $P$ | $P/P_{SHV}$ | Sequence |
|---|---|---|---|---|
| J051709.4−695927 | 136 | 98.9 | 0.73 | C |
| J053005.8−702407 | 186 | 110.0 | 0.59 | C/B |
| J052642.1−693522 | 169 | 127.0 | 0.75 | C/B |
| J051817.5−695857 | 264 | 137.7 | 0.52 | C/B |
| J052550.4−695112 | 432 | 161.4 | 0.37 | D/B |
| J051812.4−693748 | 129 | 254.0 | 1.97 | C/E |
| J050940.5−692416 | 169 | 336.2 | 1.99 | C/E |

On the other hand, because the ratios of two periods for the stars J053005.8−702407, J051817.5−695857, J051812.4−693748 and J050940.5−692416 are close to 1 : 2, the uncertainty can be due to case 2 (Section 3.3). The light curves of the stars J051812.4−693748 and J050940.5−692416 are likely Period 2 oscillation (see Appendix B). The stars J051709.4−695927 and J052642.1−693522 show the period ratio around 4 : 3, which indicates a transition between Period 4 oscillation and a harmonic mode. For the star J052550.4−695112, the period (161.4 d) obtained in the present study is plausible although the period (432 d) adopted by Hughes & Wood (1990) exceeds the time-span of the MOA observation. If both determinations are correct, a period ratio of 1 : 3 suggests a transition to one of the harmonic modes.

Here it is worth noting that the non-linear nature of the oscillation (case 2) may produce a ghost sequence in the period–luminosity relation. It is important that such a ghost sequence would come from the essential property of pulsating stars in the RGB, not from the failure or incompleteness of the numerical analyses. Because twice the period of the enhanced mode can be obtained in the case 2 ambiguity, sequence E could be a ghost sequence of the richest sequence, sequence C.

SR variables change their period frequently. The semiregularity is explained connected with the random changes of oscillatory motion caused by the imperfection of reflection at the stellar surface. Such a scheme does not match the sequential structure characterized by the simple period ratios in the period–luminosity diagram and the period transition between the separated sequences.

Recently, Kiss et al. (1999) analysed the variability of 93 SR variables and found that most of them vary with two or more periods. This type of multiperiodicity of the LMC variables has been reported by Wood (2000). The period ratio found by Kiss et al. (1999) is in the range from 1–1.78 to 2 or from 0.56–0.5 to 1 in most cases. This implies resonant enhancement of the lower or higher harmonics and also implies the existence of the Period 2 oscillation. Careful analysis of the non-linear feature of light curves is required to distinguish an enhancement of the harmonics and a period-doubling.

## 5 COLOUR DEPENDENCY

### 5.1 CMD with $V_m$ and $R_m$

Fig. 11 shows the ($\langle V_m\rangle$–$\langle R_m\rangle$, $\langle V_m\rangle$) plot for 17 530 stars which are selected from the MOA data base at random. They include non-variable stars. In Fig. 11, the TRGB is located at ($\langle V_m\rangle$–$\langle R_m\rangle$) $\approx$ 1.2 mag and $\langle V_m\rangle \approx 17$ mag. The AGB extends to the red region beyond ($V_m$–$R_m$) $> 1.2$.

Fig. 12 shows the same CMD for the stars in each sequence. Their colours are very red and beyond the tip of the RGB compared with Fig. 11, which indicates that the selected variables are mostly AGB stars.

Alcock et al. (2000) indicated in their fig. 7 that their 11 variables belong to two groups (bright and faint stars) in the quantity $W_{2.0} = V - 2.0\,(V–R)$. They suggested that the variables fainter in $W_{2.0}$ are old and metal-poor.

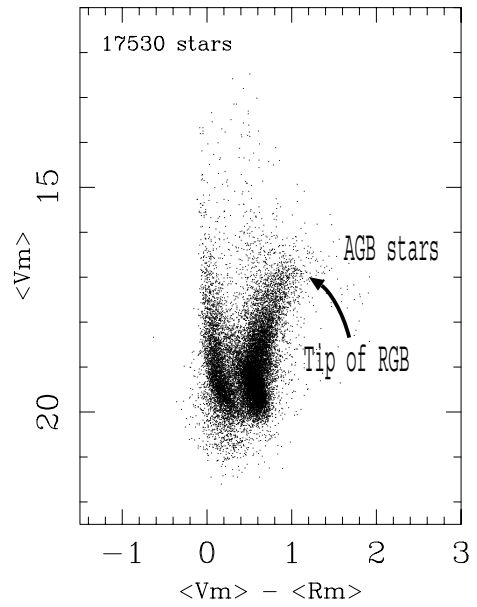


**Figure 11.** CMD ($\langle V_{\rm m}\rangle$–$\langle R_{\rm m}\rangle$) versus $\langle V_{\rm m}\rangle$ for 17 530 stars.

The regression fitting for our variables in all sequences yields the relation

$$\langle V_{\rm m}\rangle = 1.17(\langle V_{\rm m}\rangle - \langle R_{\rm m}\rangle) + 15.32. \quad (3)$$

We examined 917 variables selected by the colour cut, $1.1 < \langle V_{\rm m}\rangle$–$\langle R_{\rm m}\rangle < 1.3$, and found a bimodal distribution whose peaks are located at $\langle V_{\rm m}\rangle - 1.17$ ($\langle V_{\rm m}\rangle$–$\langle R_{\rm m}\rangle$) $\approx$ 15.2 and 15.6. The variables of sequences A, B, and C are distributed in both regions while those of sequences D and E are found only in the fainter part.

### 5.2 CMD with $R_{\rm m}$ and $K_{\rm S}$

The colour ($\langle R_{\rm m}\rangle$–$K_{\rm S}$) is a better indicator of the effective temperature of the stars than ($V_{\rm m}$–$R_{\rm m}$) colour, because our $V_{\rm m}$ covers the standard $B$ band which is seriously affected by the carbon-to-oxygen ratio. In fact, the comparison of 16 oxygen-rich (M-type) variables and 12 carbon-rich (C-type) stars based on the MOA and the DCMC shows a clear separation between the two types on the ($\langle V_{\rm m}\rangle$–$\langle R_{\rm m}\rangle$, $\langle R_{\rm m}\rangle$–$K_{\rm S}$) diagram, as shown in fig. 14 of Paper I. The relation between the oxygen-rich or carbon-rich and each period–luminosity sequence will be discussed in Section 6.1.

Fig. 13 shows the CMD ($\langle R_{\rm m}\rangle$–$K_{\rm S}$, $K_{\rm S}$) of each sequence. Note that, even though the colour ($\langle R_{\rm m}\rangle$–$K_{\rm S}$) may be not so accurate because $K_{\rm S}$ is a single-epoch observation, the ($\langle R_{\rm m}\rangle$–$K_{\rm S}$, $K_{\rm S}$) diagram is interesting to estimate the relation of the bolometric magnitude

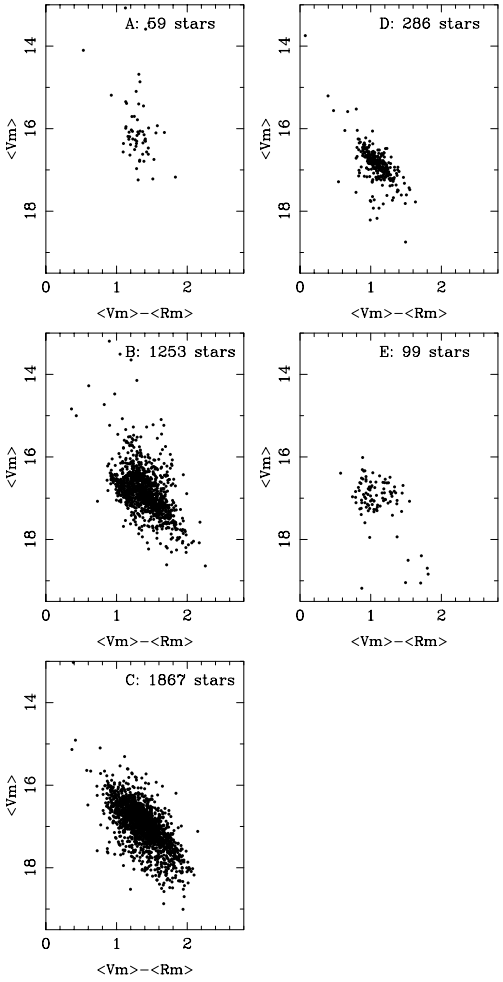


**Figure 12.** CMD ($\langle V_{\rm m}\rangle$–$\langle R_{\rm m}\rangle$) versus $\langle V_{\rm m}\rangle$ of the stars in each period–magnitude sequence.

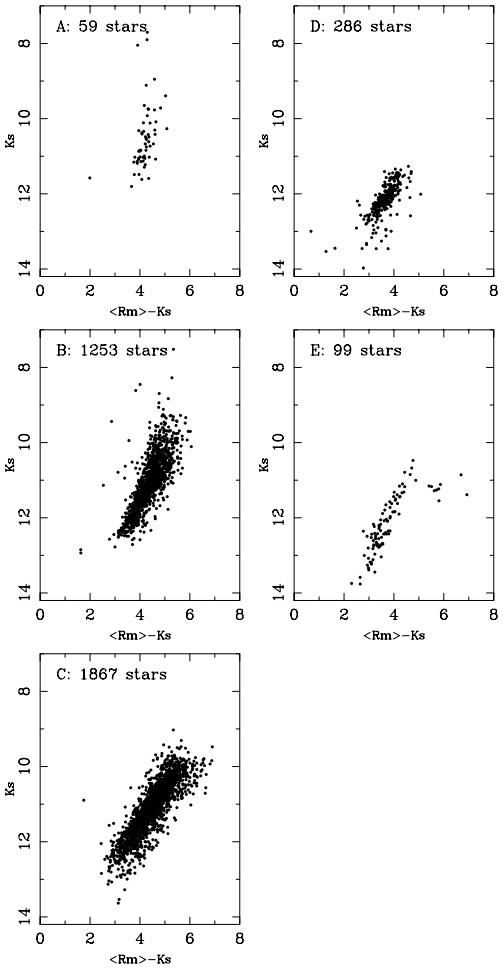


**Figure 13.** CMD ($\langle R_{\rm m}\rangle - K_{\rm S}$) versus $K_{\rm S}$ of the stars in each period–magnitude sequence.

**Table 4.** Mean position of five sequences on the CMD. Gradient is $dK_S/d(\langle R_m\rangle - K_S)$.

| Sequence | Brightness $K_S$ (mag) | Colour $(\langle R_m\rangle - K_S)$ (mag) | Gradient |
|---|---|---|---|
| A | 10.5 | 4.2 | −1.15 |
| B | 11.0 | 4.4 | −1.03 |
| C | 11.1 | 4.5 | −0.82 |
| D | 12.2 | 3.6 | −0.65 |
| E | 12.2 | 3.8 | −0.70 |

to the effective temperature. Most of the stars are located on the AGB indicated in Fig. 2. The variables scattered outside of the giant branch reported in Alves et al. (1999) were unseen. This is because variables of less regular or too small amplitude (<0.1 mag) were excluded in our analysis.

Whereas the variable stars are distributed in a narrow area of the CMD, the five sequences are slightly separated. The mean brightness and colour of each sequence are tabulated in Table 4 together with their gradient in the CMD. The mean brightness of sequences A, B and C coincides with the major clump of the $K_S$ distribution shown in Fig. 3. On the other hand, the stars of sequences E and D are distributed in the minor clump. On the CMD, sequence A stars are located to the blue and bright side of stars of sequence B, those are located to the blue and bright side of sequence C stars. Several stars of sequence E are found apart from the main body. Stars of sequences D and E have on average a faint $K_S$ magnitude. They may be part of the faint bump indicated in Fig. 3. Their position on the $(\langle R_m\rangle - K_S, K_S)$ diagram is close to the TRGB.

### 5.3 Effect of the single-epoch observations

We used the mean brightness $\langle R_m\rangle$ derived from more than several tens of photometric observations, while $K_S$ was given by the single-epoch observations. We put $\Delta K_S$ as

$$\Delta K_S = K_S - \langle K_S\rangle, \tag{4}$$

where $K_S$ is the magnitude given in the DCMC. As we used $K_S$ instead of $\langle K_S\rangle$, the $(\langle R_m\rangle - K_S)$ values were shifted from the proper position indicated by $(\langle R_m\rangle - \langle K_S\rangle)$. When $\Delta K_S$ is positive, $(\langle R_m\rangle - K_S)$ is decreased from the proper value, so that the position on the CMD moves to a fainter and bluer position than the proper position. The gradient of such a move is −1 because

$$\partial K_S/\partial(\langle R_m\rangle - K_S) = -1. \tag{5}$$

As we have indicated in Table 4, the gradient of each sequence was close to −1. Hence, the effect of the single-epoch observation on the CMD made the scatter along the sequences. The averaged position of each sequence on the CMD was not affected by the single-epoch observations.

### 5.4 Period–colour diagram

The period–colour $(\langle R_m\rangle - K_S)$ diagrams (Fig. 14) show that the whole variable stars form five parallel strips, as in the period–magnitude diagram. Sequence D stars are the reddest. Some stars in sequence E are separated from the main body, which is just similar to the appearance of the CMD (Fig. 13). These red stars are classified into sequence E based on the position on the period–luminosity diagram, but show a different $(\langle R_m\rangle - K_S)$ colour as well.

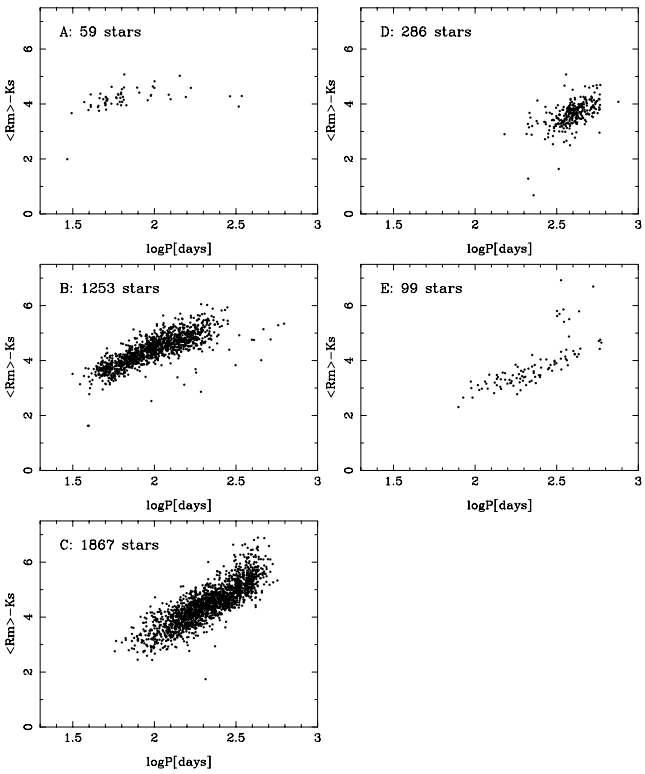


**Figure 14.** Period–colour diagram of the stars in each period–magnitude sequence. The horizontal axis is log $(P)$, where $P$ is the period in days, while the vertical axis is $(\langle R_m\rangle - K_S)$.

We point out the similarity of the Galactic short-period SRs, which are separated from the Mira sequence on the period–colour diagram (Whitelock & Feast 2000), with our short-period sequences, sequences A and B.

## 6 DISCUSSION

### 6.1 C-rich and O-rich stars

The spectral features of late-type stars can be divided into two groups: oxygen-rich (O-rich) and carbon-rich (C-rich) stars. The difference in chemical composition of the stellar atmospheres causes a difference in the spectral energy distribution, i.e. the colour derived from the photometric data. This is remarkable in the Johnson $B$ band which is included in the MOA blue band. This was shown in Paper I.

Such a property causes the duplicity of the log $P$–$(\langle V_m\rangle - \langle R_m\rangle)$ diagrams of each sequence. In Fig. 15, sequences B and C are divided into two parallel subsequences. This can be explained by the coexistence of the O-rich and the C-rich stars in these sequences. For sequences A, D and E, it is difficult to see the duplicity.

The distribution of the stars on the $(J-K, K)$ diagram has been used by many authors to distinguish O-rich and C-rich stars. The $(J-K_S)$–$K_S$ diagram of each sequence is shown in Fig. 16. Cioni et al. (2001) studied the $(J-K_S, K_S)$ diagram of the DCMC, and they discriminate the two types at $J-K_S = 1.5$ ($J-K_S < 1.5$ for O-rich stars). We examined 80 stars classified by Hughes & Wood (1990) using $J$ and $K_S$ data of the DCMC (see the bottom-right panel in Fig. 16). Most C-rich stars show large $(J-K_S)$, and only one O-rich star is redder than $(J-K_S) = 1.5$. We may use this value

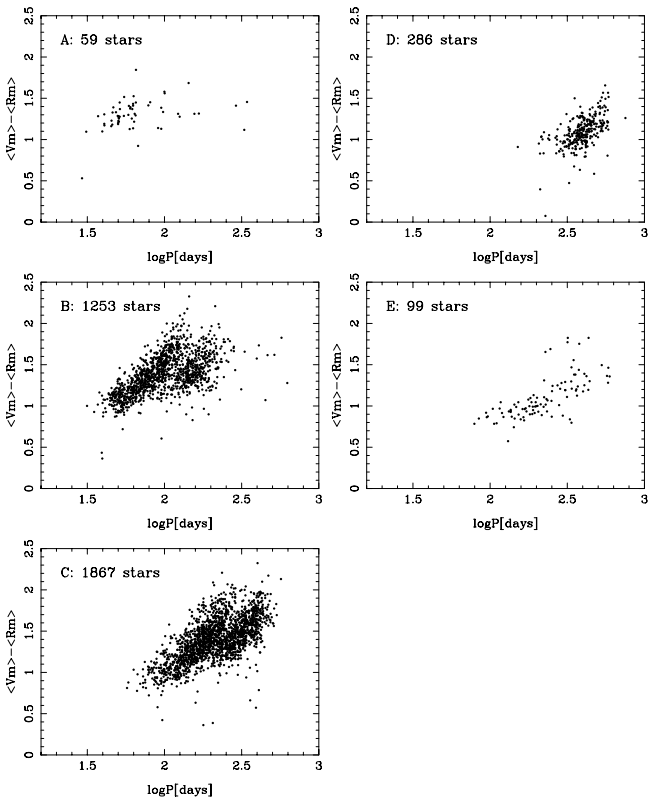


**Figure 15.** Period–colour diagram log $P$–($\langle V_{\rm m}\rangle$–$\langle R_{\rm m}\rangle$) of the stars in each period–magnitude sequence.

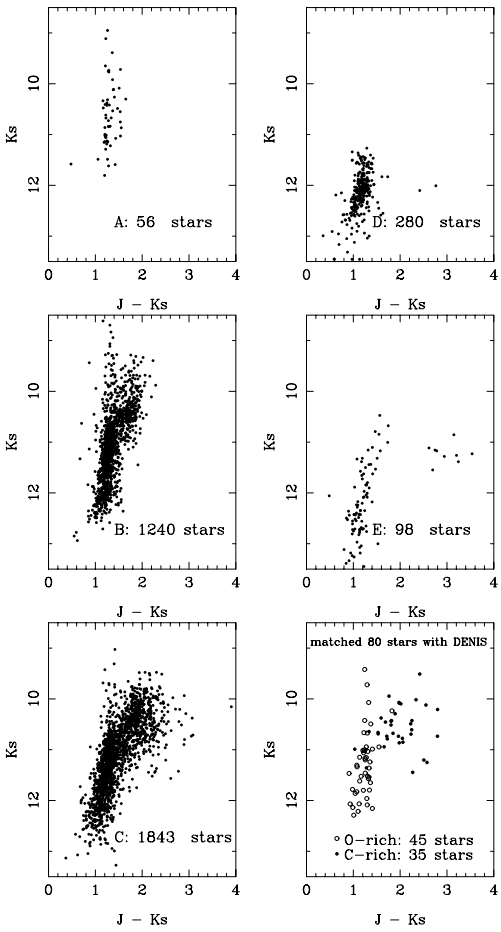


**Figure 16.** NIR CMD of the stars in each period–magnitude sequence. The horizontal axis is ($J$–$K_{\rm S}$), and the vertical axis is $K_{\rm S}$. The bottom-right panel indicates the same diagram with 80 known O-rich and C-rich stars (see text).

as the criterion for O-rich stars. In Fig. 16, some stars of sequences B and C are probably C-rich.

We summarize the correlation of the O-rich and the C-rich stars in each sequence as follows. Sequence B and C stars consist of O-rich and C-rich stars, while the majority of sequence A, D and E stars are O-rich stars. It is not confirmed yet that the difference between sequence A, B and C and sequence D and E stars is related to the difference in the chemical composition.

### 6.2 Origin of the variability

Although the Mira stars were discovered a long time ago, the pulsation mechanism is still unresolved. The confirmation of the multiplicity of the period–luminosity relation and a study of the photometric properties of the members of each sequence will help to elucidate the enigma about the AGB variables.

#### *6.2.1. Theoretical results*

Recent theoretical studies on long-period variables showed two important results.

The excitation mechanism of the Mira stars has been studied by Xiong, Deng & Cheng (1998). They succeeded in showing that the pulsational instability is caused by a different mechanism from the $\kappa$-mechanism. In their theory, they consider the delay of heat transfer caused by large-scale convection. The coincidence of the characteristic time-scale $t_{\rm D}$ and the time-scale of the stellar pulsation $t_{\rm P}$ enhances the stellar pulsation.

A large shift of the pulsation period $t_{\rm P}$ has been reported in the hydrodynamic models for the Mira stars (Ya'ari & Tuchman 1996; 1999). Even though theoretical periods of linear pulsation were studied by many authors and are in good agreement, it seems difficult to compare them directly with the observational periods (Barthés & Luri 2001).

#### *6.2.2 Multiplicity of the periods*

The discovery of the multiplicity of the period–magnitude relation is interesting because it suggests an enhancement of the overtone and/or harmonic modes. First, we confined our analysis to the variables comprising the bright clump of Fig. 3. We found three sequences in this clump. The stars of sequence C are the main component of this group. The large-amplitude and regular variables, certainly the classical Mira stars, belong to this group. The duplicity of the period–magnitude relation is clear, as shown in Fig. 4, even though sequence A was not so evident compared with sequences B and C. Such a multistrip structure of the period–magnitude diagram suggests the enhancement of the overtone and/or the harmonics. The period ratio in sequences A, B and C are 0.22 : 0.46 : 1. When the harmonics are enhanced, the period ratio of 0.25 : 0.50 : 1 is expected. Even though we cannot compare this with the theoretical periods because of the uncertainty of the pulsation period $t_{\rm P}$, such ratios are hardly expected as the overtone.

*6.2.3. Long-period, faint sequences*

As for the stars of sequences D and E, Wood (2000) argued that the eclipse of binaries, the rotation of stars with large spots, obscuration by circumstellar dust, non-radial $g^-$ mode, and an extraordinary mode of oscillation yielded by the coupling with convection were possible mechanisms.

Because we have excluded eclipsing binary candidates in this paper, the eclipsing hypotheses must be eliminated. From the position of the stars in the CMD we may suppose that their variability is related to their stellar structure. Thus stellar pulsation would be a plausible explanation. The radius of these stars should be small because the luminosity is low and the colour is blue. To pulsate with a long period, the mass would be low or the pulsation parameter $Q$ would be large. Considering the fact that the periods of these variables are approximately two and three times those of sequence C stars, we may suppose that stars of sequences D and E pulsate in the subharmonic modes. These stars are likely at the TRGB and less massive at the helium flash because they are fainter in $K_S$ magnitude than most of the AGB stars. The lack of C-rich stars in the main part of these sequences also suggests a different origin. The long period of these stars is likely explained by the low-mass nature not by the enhancement of subharmonic modes.

In order to resolve the problems about the chemical composition and other surface phenomena, it would be interesting to study the spectroscopic features of these stars. Photometric observations covering a long time-span will also provide useful information to study the evolution of these variables.

*6.2.4. Speculation*

The theory of Xiong et al. (1998) gives us an interesting scheme on the pulsation of the AGB stars. Large-scale convection changes the pattern and the time of circulation ($t_C$) coupled with convective motion will be switched from time to time. If such a scheme is correct, the period transition is easily explained. The fluctuation of the time-scale of convection may enhance successively several pulsation modes. The multiplicity of the period for the same star is then expected.

## 7 SUMMARY

The MOA photometric data of 4.4 million stars in the LMC covering the time span of 2.3 yr from 1998 August were studied. A total of 313 706 stars were identified in the DCMC. Among them, 67 107 stars were observed in the $K_S$ band. The light variation of these stars was investigated by the PDMM code. The stars for which the light curve is quite regular were selected. Light curves of 395 stars which were likely to be eclipsing variables were eliminated, and finally 3967 stars were selected for a careful study of the photometric properties. Most of these quite periodic variables were found in the AGB. A major clump of variable stars was found at $K_S \approx 11.2$, and a minor clump was located at $K_S \approx 12.2$.

In Wood (2000) the multiplicity of the period–luminosity relation, with five parallel sequences, was studied. We confirmed that the majority of the variables are concentrated on the sequence including most of the Mira stars and on a neighbouring sequence. The period ratio at the same luminosity was close to 1 : 2 between the neighbouring sequences. These facts emphasize the idea that these five sequences of the period–magnitude relation would originate by temporal enhancement of harmonic or subharmonic modes of the variables which belong to the Mira sequence.

On the $(\langle V_m\rangle - \langle R_m\rangle) - \langle V_m\rangle$ diagram, the bimodal distribution of AGB variable stars suggested by Alcock et al. (2000) was found.

The properties of the stars in each period–magnitude sequence on the $(\langle R_m\rangle - K_S) - K_S$ diagram were investigated. The shorter-period sequences (sequences A and B) were located on the bluer side. This suggests that they pulsate in higher mode overtones.

Most of the large-amplitude, regular, long-period, red variables were on the period–magnitude relation presented as that of Mira stars.

The $(J-K_S, K_S)$ features of the stars in each period–magnitude sequence indicated that the majority of sequence A, D and E stars were O-rich, while sequence B and C stars consisted of both O-rich and C-rich stars.

It should be noted that many variables showing an eclipsing binary-like light curve were found on a separate period–magnitude sequence. The nature of these stars will be investigated in a further paper.

## ACKNOWLEDGMENTS

The authors owe the main part of this paper to the thesis of Dr Sachiyo Noda. One of the authors (SN) expresses her thanks to her supervisor, Professor Yasushi Muraki, for his invaluable guidance and encouragement. This work is supported by a grant-in-aid for scientific research (A) of the Japan Ministry of Education, Science, Sports and Culture, and also by the Marsden Fund of the Royal Society of New Zealand. The authors are grateful to the University of Canterbury for the support to our observations.

## REFERENCES

Alard C. et al., 2001, ApJ, 552, 289
Alcock C. et al., 2000, AJ, 119, 2194
Alves D., Basu A., Cook K. H., Welch D. L., 1999, in Chu Y.-H., Suntzeff N. B., Hesser J. E., Bohlender D. A., eds, IAU Symp. No. 190, New Views of the Magellanic Clouds. Astron. Soc. Pac., San Francisco, p. 517
Barthés D., Luri X., 2001, A&A, 365, 519
Bedding T. R., Zijlstra A. A., 1998, ApJ, 506, L47
Buchler J. R., Kolláth Z., 2001, in Takeuti M., Sasselov D. D., eds, Stellar Pulsation – Non-linear Study.. Kluwer Academic, Dordrecht, p. 185
Buchler J. R., Kovács G., 1987, ApJ, 320, L57
Buchler J. R., Kolláth Z., Cadmus R., 2002, in Riepe M. W., Boccaktti S., Kurths J., eds, Proc. AIP Conf. Vol. 622, Experimental Chaos: 6th Experimental Chaos Conference. AIP, New York, p. 61
Cioni M.-R. et al., 2000a, A&AS, 144, 235
Cioni M.-R., van der Marel R. P., Loup C., Habing H. J., 2000b, A&A, 359, 601
Cioni M.-R., Marquette J.-B., Loup C., Azzopardi M., Habing H. J., Lasserre T., Lesquoy E., 2001, A&A, 377, 945
Feast M. W., Glass I. S., Whitelock P. A., Catchpole R. M., 1989, MNRAS, 241, 375
Gieren W. P., Fouqué P., Gomez M., 1998, ApJ, 496, 17
Hughes S. M. G., Wood P. R., 1990, AJ, 99, 784
Kholopov P. N., 1985, in General Catalogue of Variable Stars. Vol. 1. Nauka, Moscow
Kiss L. L., Szatmáry K., Cadmus R. R., Jr, Mattei J. A., 1999, A&A, 346, 542
Kolláth Z., 1998, in Takeuti M., Sasselov D. D., eds, Pulsating Stars – Recent Developments in Theory and Observation. Universal Academy Press, Tokyo, p. 183
Laney C. D., Stobie R. S., 1994, MNRAS, 266, 441
Lebzelter T., Schultheis M., Melchior A. L., 2002, A&A, 393, 573
Noda S. et al., 2002, MNRAS, 330, 137 (Paper I)
van der Marel R. P., Cioni M.-R., AJ, 2001, 122, 1807

Whitelock P. A., 1999, in Ferlat R., Maillard J.-P., Raban B., eds, Variable Stars and the Astrophysical Returns of the Microlensing Surveys. Edition Frontiéres, Gif-sur-Yvette, p. 163
Whitelock P. A., Feast M., 2000, MNRAS, 319, 759
Wood P. R. et al., 1999, in Le Bertre T., Lébre A., Waelkens C., eds, IAU Symp. No. 191, Asymptotic Giant Branch Stars. Astron. Soc. Pac., San Francisco, p. 151
Wood P. R., 2000, PASA, 17, 18
Xiong D. R., Deng L., Cheng Q. L., 1998, ApJ, 499, 355
Ya'ari A., Tuchman Y., 1996, ApJ, 456, 350
Ya'ari A., Tuchman Y., 1999, ApJ, 514, L35
Yanagisawa T. et al., 2000, Exp. Astron., 10, 519

## APPENDIX A: TYPICAL LIGHT CURVES OF RED VARIABLES

Typical light curves of red variables found in the MOA data base are shown here. Fig. A1 shows the light curve of the star MOA J052929.1−693251. This is a type S, whose light curve is similar to a sinusoidal curve. The upper-left panel indicates the parameter $\theta$ of the PDMM code with the assumed period. Because the minimum value of $\theta$ is 0.48, the period was determined with good quality. The upper-right panel shows the residuals from the selected period. The middle panel shows the phase curve and the lower panel shows the periodogram. The light curve is obviously sinusoidal, but cycle-to-cycle modulation was found. Such a temporal change is typical in Mira stars.

The light curve of the star MOA J051036.1−690817 is typical of type W, a classical Cepheid with a bump on the ascending branch (Fig. A2). The phase of the bump follows the well-known Hertzsprung relation as a function of the period. The sharp drop of $\theta$ in the upper-left panel indicates the high quality of the period determination. This is because the observations cover a time range much

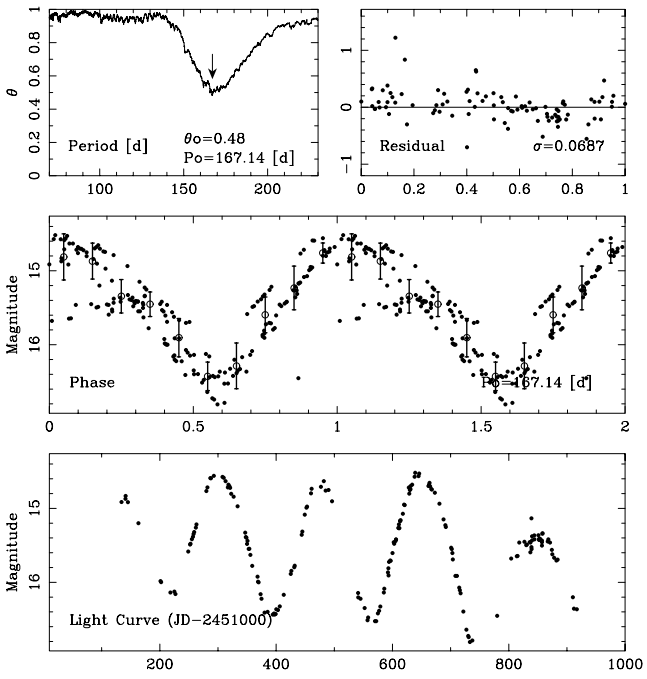


**Figure A1.** An example of type S, a light curve similar to a sinusoidal curve. The upper-left panel indicates the parameter $\theta$ of the PDMM code with the assumed period for the star MOA J052929.1−693251. The upper-right panel shows the residual of each data point from the light curve for the selected period. The middle panel is the superposed light curve by folding, and the lower panel is the photometric data.

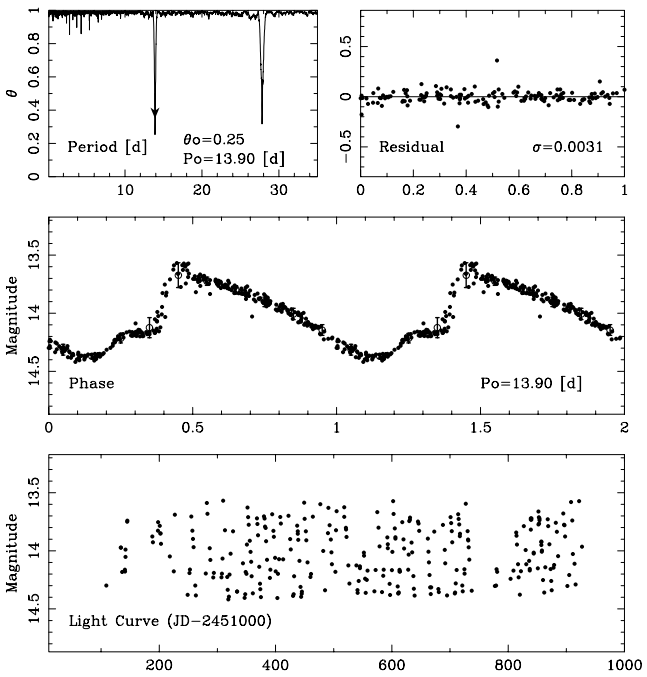


**Figure A2.** An example of a type W light curve. The sharp drop of $\theta$ in the upper-left panel shows the good quality of the period determination. The folded light curve shows that the star is a classical Cepheid. The star is MOA J051036.1−690817.

larger than the pulsation period and the oscillation is also highly stable.

The light curve of the star MOA J051904.0−692932 is a typical example of type C, which is defined by a sharp drop at the light minimum (Fig. A3). The diagram of $\theta$ (upper-left panel) shows a wide dip. This indicates the SR nature of the variability. The sharp

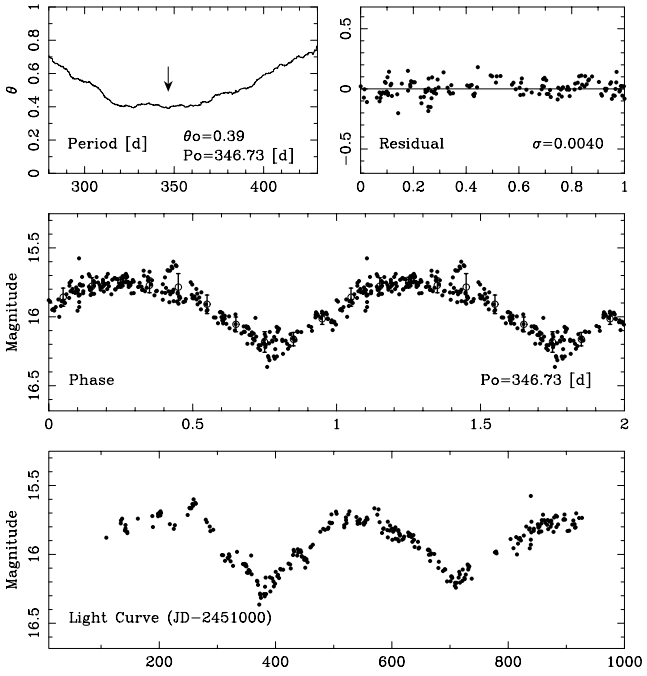


**Figure A3.** An example of a type C light curve. This type is characterized by the sharp drop and steep increase of the light minimum. The star is MOA J051904.0−692932.

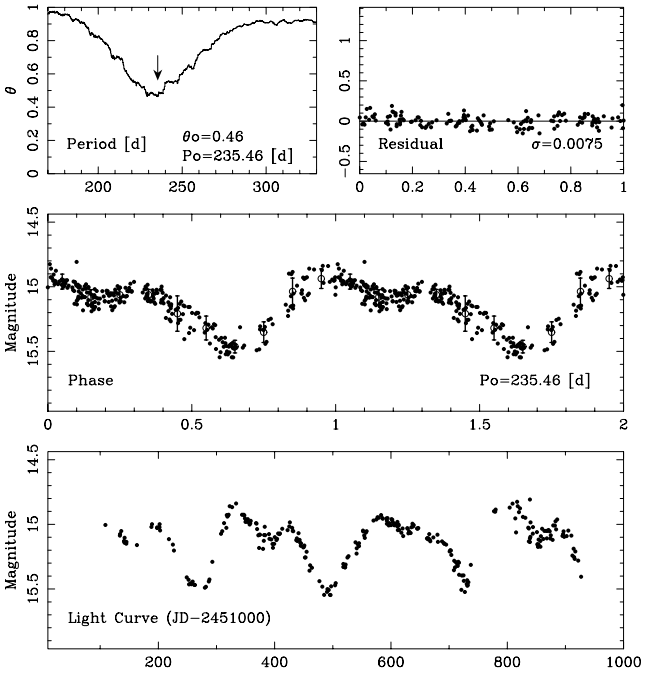


**Figure A4.** An example of an RV-Tauri-type, type T, light curve. The star is MOA J052108.5−691709.

drop and steep increase of the light minimum look like the partial eclipse in a binary system. On the other hand, SR variability is an indication of pulsation in a red giant. These stars were classified as red long-period pulsating variables.

The star MOA J052108.5−691709 is a type T variable which has the RV Tauri-like light curve (Fig. A4). These are defined by the spectral type, F–K, the period, 30–150 d, and alternating deep and shallow light minima. The star MOA J052108.5−691709 is not an RV Tauri star because the colour is too red and the period exceeds the limit. The light curve typical of the RV Tauri stars is produced by the coupling between a damping overtone mode and the first harmonic of the main mode (Kolláth 1998). The long-period variables with RV-Tauri-like light curves were also the result of the coupling with a higher mode (Buchler, Kolláth & Cadmus 2002). The discovery of many type T variables is the evidence of the 1 : 2 resonance in the AGB stars.

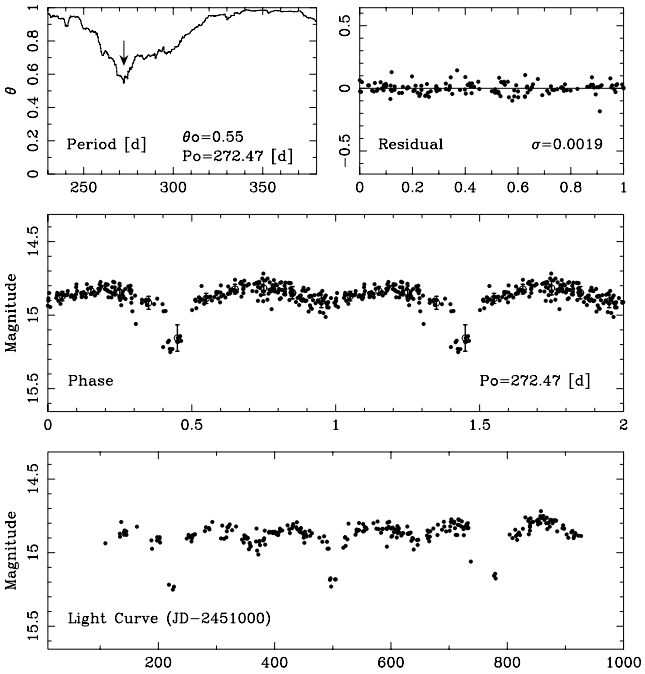


**Figure A5.** A light curve of MOA J051857.6−692954, classified as type E. It shows the features of an eclipsing variable.

The light curve of the star MOA J051857.6−692954 is like that of eclipsing variables (Fig. A5). The primary light minimum in the phase curve indicates the flat part in a total eclipse. The wide secondary light minimum with gradual light variation suggests that it is nearly a contact binary.

## APPENDIX B: AMBIGUITY OF PERIODS AND LARGE-AMPLITUDE STARS OF SEQUENCES B AND E

As described in Section 3.3 there are two effects that may lead to an incorrect determination of the period using our algorithm. First, the derived period may be too short and, secondly, it can be half or twice the real period.

The adopted period of the star MOA J050940.5−692416 was 336.21 d in the present paper, although Hughes & Wood (1990) found a period of 189 d (see Table 3). The light curve is shown in Fig. B1. Because we have four cycles of oscillation, the period-doubling nature was revealed. When the observer cannot obtain sufficient data, it is difficult to detect this feature. For another star MOA J051812.4−693748, the period of 253.97 d was adopted in the present paper; on the other hand Hughes & Wood (1990) obtained 129 d (also see Table 3). The light curve is shown in Fig. B2. These light curves show alternating high and low light maxima very similar to those obtained in a theoretical paper (Ya'ari & Tuchman 1996).

When we take the period-doubling bifurcation caused by strong non-adiabaticity possibly working in the AGB variables into account, the period of the enhanced mode will be the shortest one, such as the single period in the RV Tauri stars. For example, the

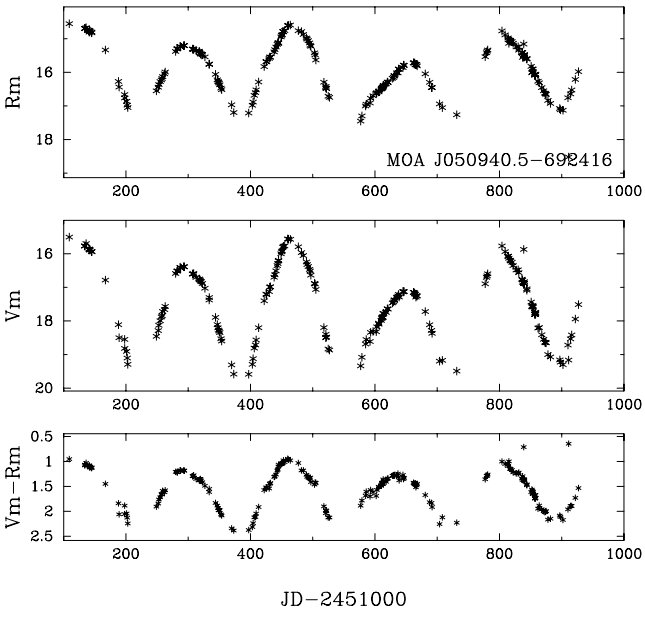


**Figure B1.** The light curve of MOA J050940.5−692416. The adopted period is 336.21 d in the present paper, while Hughes & Wood (1990) found a period of 169 d.

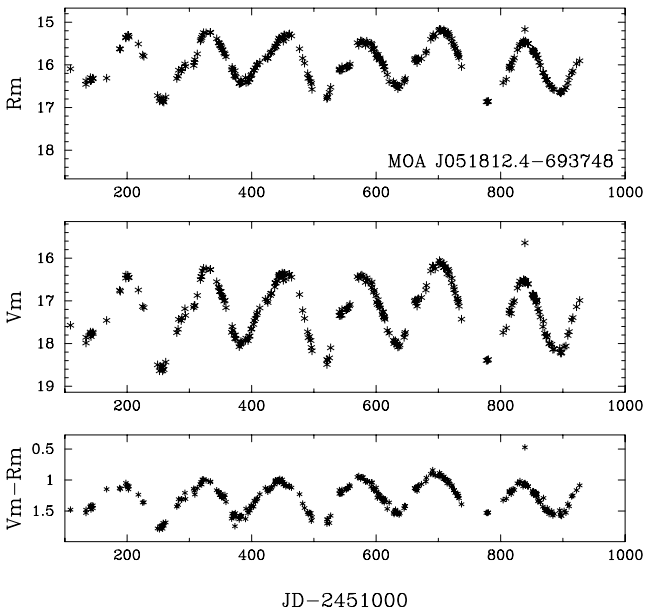


**Figure B2.** The light curve of MOA J051812.4−693748. The adopted period is 253.97 d in the present paper. Hughes & Wood (1990) obtained 129 d.

periods of these stars in the small-amplitude stage will be 168.1 and 126.5 d, respectively. The increase of the amplitude makes the non-linear effect stronger, and then the period bifurcates into two different values. The oscillations of these stars were really yielded by the period-doubling bifurcation; the oscillation indicated in Figs B1 and B2 would be Period 2 oscillation. Because the harmonic or subharmonic modes will be enhanced simultaneously, it is possible that the apparent similarity with Period 2 oscillation is not essential.

The large-amplitude variables are important because they can be used as distance indicators for extragalactic systems. We have found five large-amplitude stars in sequence B and 17 stars in sequence E. Taking into account the ambiguity of the period determination indicated above, we discuss possible changes of the membership to a given period–magnitude sequence for these stars.

The properties of the five stars of sequence B are tabulated in Table B1. The periods of three of them were too long to accept them as the final results. The other two stars were of case 2 (Section 3.3 observations are used); the three case 1 stars move to sequence C. If the period-doubling bifurcation is really working in the AGB variables, the single period will be the proper period of the system. If all of the large-amplitude stars of sequence B can be members of sequence C, there is no room to assume the Period 2 oscillation for these variables. The transition between the harmonic modes will be plausible.

**Table B1.** The ambiguity of the large-amplitude stars of sequence B. (1) is the adopted period and (2) is the possible period.

| Star MOA | Case | $P$ (d) | | Sequence |
|---|---|---|---|---|
| | | (1) | (2) | |
| J052317.6−692648 | 2 | 175.7 | 351.4 | Probably C |
| J052836.6−692003 | 1 | 573.7 | – | Possibly C |
| J050428.5−681836 | 1 | 408.2 | – | Possibly C |
| J052511.4−684244 | 2 | 246.5 | 493.0 | Probably C |
| J053700.3−671025 | 1 | 396.3 | – | Possibly C |

**Table B2.** The ambiguity of the large-amplitude stars of sequence E. (1) is the adopted period and (2) is the possible period.

| Star MOA | Case | $P$ (d) | | Sequence |
|---|---|---|---|---|
| | | (1) | (2) | |
| J050940.5−692416 | 2 | 336.2 | 168.1 | Probably C |
| J051504.9−693603 | 2 | 315.0 | 157.4 | Probably C |
| J051645.0−691952 | | 350.0 | | E |
| J051809.0−691941 | | 347.5 | | E |
| J051812.4−693748 | 2 | 254.0 | 126.9 | Probably C |
| J051534.1−684515 | | 329.2 | | E |
| J052344.6−702503 | | 189.6 | | Probably E |
| J052528.2−695828 | | 318.4 | | E |
| J053351.2−700713 | 1 | 573.0 | – | Possibly D |
| J050101.3−683339 | 1 | 594.4 | – | Possibly D |
| J050222.7−683414 | 1 | 529.2 | – | Probably D |
| J052426.6−710206 | 2 | 377.9 | 755.8 | Possibly C |
| J053252.5−714637 | | 317.5 | | E |
| J053213.5−713604 | | 246.0 | | E |
| J045633.1−681954 | | 235.4 | | E |
| J051100.2−673843 | 2 | 362.0 | 181.0 | Probably C |
| J053337.1−680600 | 2 | 228.2 | 456.4 | Possibly D |

The 17 large-amplitude stars of sequence E are tabulated in Table B2. Three of them were of case 1, and six stars were of case 2. Some of them were likely to be members of sequences C and D, and the others were located between sequences C and D. It should be noted that at least several large-amplitude variables were located between these two sequences after considering the ambiguity of the period determination.

## APPENDIX C: SYNCHRONIZATION BETWEEN PULSATION AND CONVECTION

Stars at the red side of classical Cepheids do not pulsate because convection makes the temperature gradient less steep inside the stars and hence stabilizes pulsation. Only in the case where convective elements delay the heat flux appropriately to enhance pulsation, the stars pulsate and are observed as variables. The pulsation mechanism for red long-period variables can be modelled as the synchronization of convective motion and pulsation. Xiong et al. (1998) applied the theory to model Miras and succeeded in showing the presence of an instability strip for red variables. Because the calculation is sophisticated and delicate, we try to derive the relation between the mass, the radius and the temperature of these stars with simplified assumptions. The period–luminosity relation and the sequence on the CMD will be examined.

In classical Cepheids, the pulsation is excited by the $\kappa$-mechanism for which the condition is restricted by the combination of the effective temperature and the surface gravity. On the other hand, the red giant instability strip may originate by the synchronization between pulsation and convection. The condition for pulsational instability may be given by comparing the period of possible pulsation and the effective time-scale of convective motion.

Convection is driven by the buoyancy $f_{\rm B}$ which comes from the difference of the density of a gas element, $\Delta\rho$, with the mean density of gas surrounding the element. Because the pressure difference in the gas is smoothed with the time-scale of the propagation of sound, the density variation will be maintained by the temperature variation $\Delta T$.

Then we have

$$f_{\rm B} = g\Delta\rho = \frac{g\rho\Delta T}{T}. \tag{C1}$$

The equation of motion for such a buoyancy force is

$$\frac{{\rm d}^2 r}{{\rm d}t^2} = g\frac{\Delta T}{T}. \tag{C2}$$

Estimates of the time-scale $\tau$ for passing through the convective layer whose thickness is $\Lambda$, and the maximum velocity $v_{\rm max}$ of the element are

$$\tau \approx \left(\frac{2\Lambda T}{g\Delta T}\right)^{1/2}, \tag{C3}$$

and

$$v_{\rm max} \approx \frac{g\Delta T}{T}\frac{\tau}{2} = \left(\frac{g\Lambda\Delta T}{2T}\right)^{1/2}, \tag{C4}$$

respectively.

The size of convective elements is so large that the flow cannot be laminar in the stellar interior, so that the convective flow decays into smaller convective elements. In such a case, the velocity of motion could not exceed a limit restricted by the sound velocity $c$. The exact ratio of $v_{\rm max}/c$ cannot be calculated because of the lack of a detailed theory of turbulent motion. Only we may have a condition,

$$\frac{v_{\rm max}}{c} \propto \left(\frac{g\Lambda}{T}\frac{\Delta T}{T}\right)^{1/2}, \tag{C5}$$

assuming the general condition of turbulent decay.

Then we have

$$\frac{\Delta T}{T} \propto \frac{T}{g\Lambda}. \tag{C6}$$

Equation (C6) is useful to estimate $\Delta T/T$. The time-scale of a convective element $\tau$ is written as

$$\tau \propto \left(\frac{\Lambda}{g}\frac{g\Lambda}{T}\right)^{1/2} = \left(\frac{\Lambda^2}{T}\right)^{1/2}. \tag{C7}$$

The equation expresses that the time-scale is long for thick convective layers and also for cool layers.

On the other hand, the period of stellar pulsation $P$ which is determined by the pulsation equation of a star must have a relation with the stellar radius $R$ and the stellar mass $M$. The relation is the period–density relation as

$$P \propto \left(\frac{R^3}{M}\right)^{1/2}. \tag{C8}$$

The periods of proper modes are calculated with this relation.

We have assumed that the pulsational instability of red giant stars will be caused by the synchronization of pulsation and the motion of convective elements. When the equation $n\ \tau \approx mP$ is satisfied, the pulsation will be enhanced. $n$ and $m$ are integers, but may not be larger than 1. When we assume an appropriate value for $n : m$, we have

$$\frac{\Lambda^2}{T} \approx \frac{R^3}{M} \times {\rm const.} \tag{C9}$$

It will be natural to assume that $\Lambda \propto R$, and then we have

$$M \propto RT. \tag{C10}$$

In these three physical quantities, the relative change of the representative temperature $T$ is restricted in a narrow range but the mass $M$ and the radius $R$ vary considerably depending on the evolutionary stage. So, the star of a given mass falls in the pulsationally instability strip as the stellar radius reaches an appropriate value. Equation (C10) expresses that a massive star pulsates at the luminous stage.

The period–density relation, equation (C8), and the condition of synchronization, equation (C10), yield the following relation:

$$P \propto \left(\frac{R^3}{M}\right)^{1/2} \propto \left(\frac{R^2}{T}\right)^{1/2} \propto \left(\frac{L}{T^5}\right)^{1/2}. \tag{C11}$$

The relation can be written as

$$\log L = 2\log P + 5\log T + {\rm const.} \tag{C12}$$

Thus we have the relation between the period, the luminosity, and the temperature of red giants.

The period–luminosity relation is also obtained from observations, but it is difficult to estimate the effective temperature scale of AGB stars. We assume the relation as $L \propto T^{\alpha}$ for the red long-period variables.

For Mira stars, we have as the observational result

$$\log L = 1.54\log P + {\rm const.} \tag{C13}$$

This equation can be satisfied when

$$\alpha = -17, \tag{C14}$$

in the luminosity–temperature relation. This means that a luminosity increase of 2.5 mag corresponds to a temperature decrease of 15 per cent. The temperature we used in the calculation is the representative temperature of convection layers, and will be proportional to the effective temperature of the atmosphere. We may conclude that our crude assumption of the synchronization agrees with the observational relations.

Oscillations are coupled with many other overtones and harmonic modes, so that the number of possible enhanced modes will be large. The observational results indicate that the most strongly enhanced mode yields the sequence C, and the higher harmonics are enhanced for the stars of the luminous clump. The stars of the less luminous clump pulsate in subharmonic modes of the mode enhanced in the sequence C.

It is obvious that the time-scale of convection changes with its multidimensional properties. The periods of enhanced modes affected by modal coupling shift from the proper periods derived from linear calculations. The changes of observed periods will be useful to elucidate the complicated structure of such a multiperiodic scheme.

This paper has been typeset from a TEX/LATEX file prepared by the author.